Int. J. Multiphase Flow Vol. 18, No. 6, pp. 1061–1075, 1992
Printed in Great Britain.

0301-9322/92 $5.00 + 0.00

TRANSLATION AND ROTATION OF SPHERES SETTLING IN SQUARE AND CIRCULAR CONDUITS: EXPERIMENTS AND NUMERICAL PREDICTIONS

V. ILIC,[1] D. TULLOCK,[1], N. PHAN-THIEN[1] and A. L. GRAHAM[2]
[1]Department of Mechanical Engineering, University of Sydney, NSW 2006, Australia
[2]Los Alamos National Laboratory, Los Alamos, NM 87545, U.S.A.

(Received 25 February 1992; in revised form 15 July 1992)

Abstract—The terminal settling velocities and rotation rates of spherical particles settling in circular and square conduits were investigated experimentally and numerically with the aim to benchmark the numerical predictions using the boundary element method. Spheres were allowed to settle in viscous Newtonian fluid under conditions such that only hydrodynamic forces exerted an appreciable effect. The terminal settling velocities and the rotation rates were measured as a function of the size and density of the falling sphere, the drop position of the sphere in the conduit and the dimensions and geometry of the containing vessel or conduit. The experimental measurements were subjected to an exacting error analysis and compared with fully three-dimensional boundary element calculations. We found that the results of the experiments and numerical simulations showed remarkable agreement within the bounds of experimental error.

Key Words: falling sphere, sphere, cylinders, square conduits, rotation, wall correction factor, drag, Stokes' law

INTRODUCTION

Stokes (1851) provided an exact analytical solution for a sphere settling in an unbounded Newtonian fluid at zero Reynolds number. The result is known today as Stokes' law (e.g. Bird *et al.* 1960). The terminal velocity of the sphere, U_t, is given by

$$U_t = \frac{2a^2(\rho_p - \rho_f)g}{9\mu_f}, \qquad [1]$$

where a is the radius of the sphere, ρ_p is the density of the falling sphere, g is the gravitational constant, and ρ_f and μ_f are the density and viscosity of the Newtonian fluid, respectively. Stokes' problem is somewhat artificial, as Brenner and his coworkers (Brenner 1962; Pliskin & Brenner 1963) have shown that bounding walls have an effect on the solution even when the bounding walls are at infinity. Although the effect of bounding walls has been the subject of numerous investigations (Happel & Brenner 1986) following Faxén (1921) initial reflection solutions, various computational and experimental difficulties have prevented a complete investigation of the problem. This study considered wall and end effect for spheres settling through Newtonian fluids in circular and square conduits. Careful experiments and fully three-dimensional boundary element calculations of terminal settling velocities and rotation rates were performed for spheres settling along the centerline and eccentrically in the conduits over a wide range of experimental parameters.

Spheres settling along the centerline in circular cylinders have been the subject of many theoretical, numerical and experimental studies. For example, Ladenburg (1907), Bacon (1936) and Fidleris & Whitmore (1961) reported on generally careful experiments measuring the terminal velocity of spheres settling along the centerline of circular cylinders far from the upper free surface and fixed end of the container. Eulerian and Lagrangian flow visualization around a sedimenting sphere settling in a circular cylinder was reported in Coutanceau (1968, 1987). Coutanceau (1971a,b) also obtained a wall correction for a sphere settling along the axis of a circular cylinder. Following Faxén's reflection solution to account for the presence of circular containing walls in an infinite tube, there have been numerous attempts to extend his work. A good review of the

analytical efforts to account for the presence of the containing walls was given by Happel & Brenner (1986). This problem has also received a greal deal of attention from the numerical modelling community (e.g. Graham *et al.* 1989; Lunsmann *et al.* 1989; Zheng *et al.* 1990). Aside from extending the results to very large spheres, the inclusion of these results in this study was primarily for benchmarking our techniques.

Reported experimental data for square containers at low Reynolds numbers, appear to be limited to terminal velocities of spheres falling along the centreline of square containers (Miyamura *et al.* 1981). Tachibana (1973) also considered settling spheres in a square cylinder, but at a minimum sphere Reynolds number of about 7. Analytical studies (Happel & Bart 1974) have been performed for small spheres by a reflection solution. In this investigation, the computed values of the Stokes' law wall correction factor, for spheres settling along the centreline of square ducts, were compared with Miyamura *et al.*'s (1981) results and our own experimental results which were obtained over a wider range of dimensionless sphere sizes. The numerical predictions using the boundary element method (BEM) were found to be indistinguishable from our experimental measurements over the range of our data, although they tended to be somewhat larger than Miyamura *et al.*'s results for very large dimensionless spheres.

Spheres settling off the centreline, or eccentrically, in circular and square conduits have received more limited attention. Tözeren (1982) calculated torque on eccentric spheres falling in tubes. Experimental observations by Craig (1951) and Bart (1959) were reported by Happel & Brenner (1986) to be unable to resolve the slight maximum in the terminal settling velocity predicted by Brenner and his coworkers (Hirschfeld *et al.* 1984) as the sphere moved outward towards the containing cylinder walls. Previous numerical studies have been unable to resolve the relatively small angular velocities associated with the off-centre drops. There appear to be no reliable measurements of the angular velocity to compare to the reflection solution results predicted by Happel & Brenner (1986) and Hirschfeld *et al.* (1984) for small spheres. As we will demonstrate, the angular velocity predictions of the BEM were, generally, in good agreement with their results for small falling spheres near the centreline. For larger spheres or spheres approaching the containing walls, qualitatively similar behaviour was observed, but the numerical predictions are considered to more accurately model the particle rotations than the analytical predictions. In square conduits, where no analytical predictions or previous experimental measurements are available, our numerical predictions and experimental measurements of the angular velocities of eccentric falls were found to be in close agreement over the entire range of our data.

Experimental data for spheres approaching the bottom of circular cylinders were given by Sutterby (1973a,b) and for larger spheres by Graham *et al.* (1989). Reflection solutions were generated by Tanner (1963) and Sonshine *et al.* (1966a,b) and were limited to small falling spheres several sphere diameters from the bottom of a circular cylinder. In this study, large falling spheres were considered settling on the centreline and eccentrically, in circular and square containing vessels. Both terminal linear and angular velocities were measured. Additionally, in this study, small and large sphere trajectories were measured in the region approaching the bottom of a square conduit along the centreline of the vessel. All experimental data were subjected to a rigorous error analysis to determine the error bars on the data.

BEM predictions were made in this paper for end effects in square conduits from a series of "quasi-static" steps (Happel & Brenner 1986). In the square conduits the end effects predicted by the BEM calculations and experimental measurements were found to be qualitatively similar.

A brief discussion of the BEM model and boundary conditions will be made in the following section, followed by a description of the experimental apparatus and technique along with data reduction procedure. A comparison of the experimental findings and BEM predictions with the available literature is the subject of the third section. The final section will summarize the conclusions and discuss the implications for future research in the area of modelling Stokes' flows with the BEM.

The overall aim of the reported work was to benchmark the BEM against the experimental data for single spheres dropped axially and eccentrically in circular and square cylinders filled with quiescent Newtonian liquid.

METHOD

BEM formulation

The BEM used to model sedimenting particles is well described by Tran-Cong & Phan-Thien (1989). An outline of the method is given here.

We are concerned here with modelling the isothermal, steady state, creeping flow of a particle through an incompressible Newtonian fluid. The governing equations and the constitutive equation are, respectively,

$$\nabla \cdot \boldsymbol{\sigma} = \mathbf{0}, \tag{2}$$

$$\nabla \cdot \mathbf{u} = 0 \tag{3}$$

and

$$\boldsymbol{\sigma} = -p\mathbf{I} + 2\mu\mathbf{D} \tag{4}$$

where $\boldsymbol{\sigma}$ is the total stress tensor or stress dyadic, $\mathbf{u}$ is the velocity vector, $\mathbf{D}$ is the rate-of-deformation tensor, μ is the viscosity, p is the hydrostatic pressure that arises due to the incompressibility constraint [3] and $\mathbf{I}$ is the unit tensor. The boundary traction field is defined by

$$\mathbf{t} = \mathbf{n} \cdot \boldsymbol{\sigma}, \tag{5}$$

where $\mathbf{n}$ is the unit normal vector pointing outwards from the fluid domain.

The set of equations [2]–[4] is recast in integral form by using a method involving weighted residuals (Bush & Tanner 1983), or by making use of Betti's reciprocal theorem (Banerjee & Butterfield 1981). The details are not repeated here, only the resultant boundary integral equation (BIE), given as

$$C_{ij}(\mathbf{x})u_j(\mathbf{x}) = \int_{\partial\mathscr{D}} u_{ij}^*(\mathbf{x}, \mathbf{y})t_j(\mathbf{y})\,\mathrm{d}\Gamma(\mathbf{y}) - \int_{\partial\mathscr{D}} t_{ij}^*(\mathbf{x}, \mathbf{y})u_j(\mathbf{y})\,\mathrm{d}\Gamma(\mathbf{y}), \tag{6}$$

where $\partial\mathscr{D}$ is the boundary of the solution domain $\mathscr{D}$, $\mathbf{y} \in \partial\mathscr{D}$, $u_j(\mathbf{y})$ is the j-component of the velocity at $\mathbf{y}$, $t_j(\mathbf{y})$ is the j-component of the boundary traction at $\mathbf{y}$, $u_{ij}^*(\mathbf{x}, \mathbf{y})$ is the i-component of velocity field at $\mathbf{x}$ due to a "Stokeslet" in the j-direction at $\mathbf{y}$ and $t_{ij}^*(\mathbf{x}, \mathbf{y})$ is its associated traction. Here $C_{ij}(\mathbf{x})$ depends on the local geometry: $C_{ij}(\mathbf{x}) = \delta_{ij}$ if $\mathbf{x} \in \mathscr{D}$ and $C_{ij}(\mathbf{x}) = \frac{1}{2}\delta_{ij}$ if $\mathbf{x} \in \partial\mathscr{D}$ and $\partial\mathscr{D}$ is a smooth surface. Details of $u_{ij}^*(\mathbf{x}, \mathbf{y})$ and $t_{ij}^*(\mathbf{x}, \mathbf{y})$ for three-dimensional and half-space problems are given elsewhere (cf. Brebbia *et al.* 1984). If the particle is rigid, then a further simplification of [6] is possible (Youngren & Acrivos 1975; Tran-Cong & Phan-Thien 1986). However, a more general approach will be adopted here, as follows.

The BIE [6] can be generalized to multiconnected regions (Rizzo 1967) without much difficulty. In this case $\partial\mathscr{D} = \mathbf{S} \cup \mathbf{S}_1 \cup \cdots \mathbf{S}_\alpha$, where $\mathbf{S}$ or $\mathbf{S}_\alpha$ is the boundary of a typical singly-connected region. Either $\mathbf{u}$ or $\mathbf{t}$ must be prescribed on every part of the boundary $\partial\mathscr{D}$.

An analytical solution of [6] is not possible in general. However, if the boundary $\partial\mathscr{D}$ is divided into a series of M elements over which the geometry, velocity and traction are approximated by piecewise polynomials, an approximate solution may be obtained.

Thus, approximating velocity and traction over an element by

$$u_j = N^\alpha u_j^\alpha, \quad t_j = N^\alpha t_j^\alpha, \tag{7}$$

where N^α, $\alpha = 1, \ldots, n$, is the interpolating polynomial (shape function) and u_j is the jth component of velocity at node α, the BIE [6] in discretized form now reads

$$C_{ij}(\mathbf{x})u_j(\mathbf{x}) = \sum_{q=1}^{M} \left\{ \left[\int_{\partial R_q} u_{ij}^*(\mathbf{x}, \mathbf{y})N^\alpha\,\mathrm{d}S(\mathbf{y}) \right] u_j^\alpha - \left[\int_{\partial R_q} t_{ij}^*(\mathbf{x}, \mathbf{y})N^\alpha\,\mathrm{d}S(\mathbf{y}) \right] t_j^\alpha \right\}. \tag{8}$$

This equation, applied to a series of collocation points (usually, but not necessarily the nodal points) over the boundary, leads to a set of linear algebraic equations. Given the appropriate traction and velocity boundary conditions, these equations can be solved (by Gaussian elimination) for the remaining boundary values.

Numerical implementation

Numerical calculations were performed with an Ardent Titan workstation using a 4-byte word length. Double-precision arithmetic was used throughout, except in a disk-based Gaussian elimination solver operation to reduce memory and storage requirements. Isoparametric trilateral and quadrilateral boundary elements were used in all simulations. Typical discretizations applied to the simulations are shown in figure 1, for the case of sedimentation of a single sphere in a circular cylinder.

It should be noted that the pressure was set to zero at a point on the end flow domain, to avoid an indeterminate pressure field. The latter would occur if only velocity boundary conditions were specified.

Further details of the discretization scheme and its numerical implementation using a constant boundary element are reported elsewhere (Tullock *et al.* 1992).

EXPERIMENTAL

Test conduits, their alignment and test liquid

The experiments were conducted in circular and square† conduits containing quiescent test liquid and having a closed bottom end, while the upper surface of each cylinder was open to the atmosphere. The open end accommodated a removable lid containing the test particle releasing fixture.

The circular conduit (59.15 mm bore × 380 mm deep) was made from 2.5 mm thick glass. The small square conduit (49.17 × 49.95 × 380 mm) was made from 10 mm thick polymethyl methacrylate (PMMA) sheet and, in the case of the large square conduit (201 × 200 × 900 mm) from sheets of 10 mm thick (fish tank) glass. The largest dimension in all cases indicates the approximate depth of liquid in a tank. The above square tanks will be referred to by their nominal dimensions (50 × 50 and 200 × 200 mm, respectively) in the remainder of this paper. Vertical alignment of the tanks was effected by the use of a spirit level and plumb line. The two video cameras used to record the start and finish of a settling sphere traverse, were levelled against the timing marks (in line with the centre of each lens) on each tank with the aid of an in-built spirit level. These settings were finely adjusted by comparing the picture from each camera against two orthogonal video pointer cross-hairs projected on the top of the monitor image such that the cross-hairs coincided with the horizontal timing marks and the vertical edge of the cylinder. The latter was previously aligned with the plumb line. In the case of the small square conduit, a further check of the tank alignment was provided by releasing a small sphere from a fixture at the top of the vessel into a matching hole in the bottom surface directly below.

The liquid temperature was controlled by the environmentally controlled laboratory atmosphere to within ± 1.0°C.

The test liquid was Gensil 150/12,500 dimethylpolysiloxane (silicone oil) manufactured by the Bevaloid Australia Pty Ltd. The specific gravity of this liquid was 0.974 (measured with a 900/1000 S&B Hills Pty Ltd hydrometer) and the viscosity 14.5 Pa s (measured with a PSL 1619/8 BS/U size H capillary viscometer). Both measurements were made at 20.0°C.

The basically Newtonian nature of the fluid as well as temperature dependence (in the range 10.0 to 30.0°C) of its viscosity were determined, up to shear rates of $34\,s^{-1}$, with an Instron 3250 rheometer and water-cooled Carri-Med controlled stress rotating cone rheometer, respectively. The obtained values for viscosity at 20.0°C agreed well with that obtained using the capillary viscometer.

Apparatus, data collection and processing

At the start of an experiment, the particle to be dropped was held by vacuum in the required position in the test conduit fixture lid and, in the case of eccentric drops, it was fully immersed in the tank liquid prior to its release. Two video cameras (Panasonic WV-BL200) with 420

†Purists will argue that, from the given tank dimensions, it would be more appropriate to call them rectangular. While acknowledging that, we shall still refer to them to what their nominal dimensions purport them to be, because no significant affects on our data were found for the range of experimental parameters used.

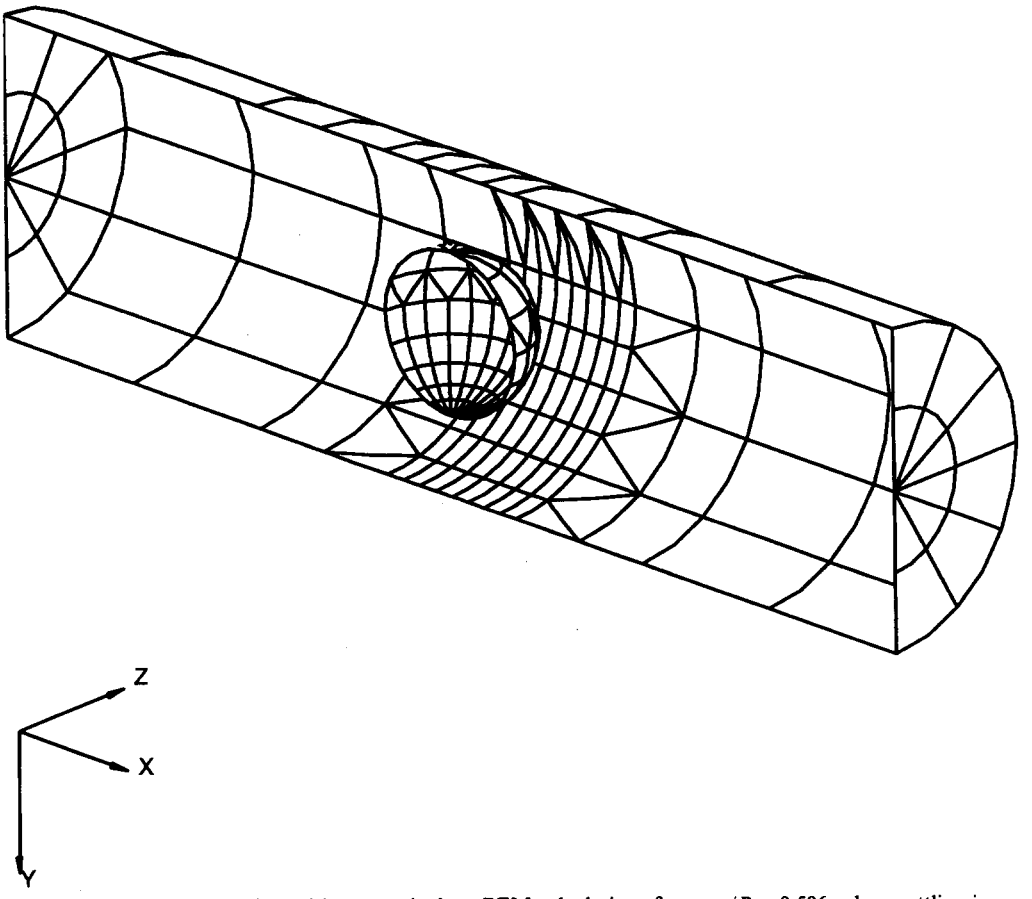

Figure 1. Typical mesh used in eccentric drop BEM calculations for an $a/R = 0.506$ sphere settling in a circular cylinder.

horizontal line resolution at the centre, were each fitted with a Computar lens ($f = 1:1.2$, 12.5–75 mm zoom) and focused, one on the top and the other on the bottom timing marker on the conduit outside walls. A video splitter (American Dynamics 1470 A) was used to provide a simultaneous view of the two images on the monitor (National WV-5410E/A) screen whose resolution was more than 850 lines at the centre. The displayed combined image was recorded on a SVHS VCR (Panasonic NVFS 100A). Superimposed on the combined image on the monitor screen image were the time (to one-hundredths of a second) and date from the National time/date generator WJ-810. The VCR was manually activated each time a particle approached the timing line such that, on tape replay, the starting and finishing time of the settling particle could be accurately determined.

The recorded image was played back on the VCR and displayed on the video monitor. With the aid of a single-frame advance and still-image facility, the time interval between the timing markers (a known distance apart) could be read off the tape, to yield the particle settling velocity. The top marker was placed far enough from the particle drop point to ensure that the terminal velocity was reached and that the bottom marker was well away from the conduit end such that no detectable end-effects were introduced.

The measurement of a particle angular velocity required the use of a video pointer (Colorado Video 610E) equipped with independently movable orthogonal cross-hair images. The pointer provided two voltage output signals the magnitude of which corresponded to the position of the cross-hair x–y coordinates on the monitor screen. This voltage signal was digitized with a PC resident, 8-bit A/D converter and its value displayed on the PC monitor for manual recording. Each sphere was marked with a black dot about 1 mm dia and oriented such that this reference mark always faced the cameras. The sphere was held by vacuum applied to a small holding cylinder, which ensured that, when suction was removed, the sphere separated without any initial

Table 1. Typical components of the fractional error in the Stokes' law wall correction factor for sedimentary spheres in square cylinders

d [mm]	$\delta H/H$	$\delta t/t$	$\delta d/d$	$\delta M/M$	$\delta\rho_f/\rho_f$	$\delta g/g$	$\delta\mu/\mu$	$\delta K/K$
1.89	0.002	0.0031	0.0074	0.0039	0.0001	2.04×10^{-7}	0.013699	0.0303
19.99	0.002	0.0031	0.0007	0.0000	0.0001	2.04×10^{-7}	0.013699	0.0197

rotation. Therefore, on a still image, it was only necessary to take three vertical pointer measurements to obtain the angular displacement of the sphere. From two sets of such measurements (one at each timing mark), the angular velocity of the particle could then be readily deduced.

Scope of the experiments

Experimental tests were restricted to evaluating the Stokes' law wall correction factor in square conduits for a range of sphere sizes (1.89–39.93 mm dia) made from steel or acetal resin (Delrin).

In addition, the effect of eccentric drops on settling and angular velocities was measured in square and circular cylinders with a 6.40 and 12.85 mm dia PMMA spheres in a square section and 6.35 mm dia ruby and 29.95 mm dia Delrin spheres in a circular tank.

The effect of the end surface on the settling velocity of a 3.15 mm dia aluminium sphere and a 29.95 mm dia Delrin sphere in a square (50 × 50 mm) tank was also determined.

Error analysis

The Stokes' law wall correction factor may be defined (e.g. Clift *et al.* 1978) as

$$K \equiv \frac{U_\infty}{U_t}, \qquad [9]$$

where U_t is the terminal velocity of a sphere diameter d and density ρ_p falling vertically in a fluid of density ρ_f whose viscosity μ_f was denoted by μ_∞ to emphasize its relationship with U_∞ obtained from the Stokes' law and applicable to an unbounded fluid.

Therefore,

$$K = \frac{d^2(\rho_p - \rho_f)g\,\Delta t}{18\mu_\infty\,\Delta H}. \qquad [10]$$

Here g denotes the local gravitational constant† ($9.796720 \pm 2 \times 10^{-6}\,\mathrm{m\,s^{-2}}$) and Δt is the time taken for a sphere to fall through a vertical distance ΔH while falling with the terminal velocity.

Following Topping (1966) and Shoemaker & Garland (1962), and denoting the mass of a sphere by M, it can be shown that the fractional error associated with K is

$$\frac{\delta K}{K} = \frac{\delta H}{H} + \frac{\delta t}{t} + \frac{1 + \dfrac{\rho_f \pi d^3}{3M}}{1 - \dfrac{\rho_f \pi d^3}{6M}}\frac{\delta d}{d} + \left(\frac{1}{1 - \dfrac{\rho_f \pi d^3}{6M}}\right)\frac{\delta M}{M} + \frac{1}{\dfrac{6M}{\pi d^3 \rho_f} - 1}\frac{\delta\rho_f}{\rho_f} + \frac{\delta g}{g} + \frac{\delta\mu_\infty}{\mu_\infty}. \qquad [11]$$

Typical values of the above fractional error are shown in table 1. As the major error component was due to the measurement of sphere size and viscosity of the tank liquid, the error tended to be greater for small spheres all else being the same.

Determination of the experimental random error associated with the evaluation of particle settling and rotational velocities was performed in a similar way. On average, the fractional error associated with a settling velocity measurement was typically $< \pm 2\%$, while the more complex measurement of the angular velocity incurred an error of around $\pm 13\%$.

The systematic error associated with the asymmetry of the square tank cross-section dimensions was found to depend on sphere size relative to the tank cross-sectional area. On this basis, the magnitude of this error was $< \pm 1\%$.

†Courtesy of H. Groeveld, CSIRO.

RESULTS AND DISCUSSION

The wall effect

The applicability of Stokes' law to the experimental data analysis was determined on the basis of negligible inertia effects reflected by the low Reynolds number ($U_t d/\nu_f$) range (0.0001–0.1070) for the spherical particles used in the tests described here.

Figure 2 and table 2 show that our data and the BEM estimate of K agree remarkably well over the whole range of $d/2L(=a/L)$, where L denotes a half-length of the square tank side. The only applicable square tube wall corrections that the authors are aware of are those of Miyamura *et al.* (1981) and Happel & Bart (1974). While the former is based on a nineteenth degree polynomial fit to their experimental data, and the latter was analytically derived, the Miyamura *et al.* (1981) correlation was in better agreement with our data, except for large values of a/L (in excess of ≈ 0.75). This seems surprising, as their test section (10×10 mm) was much smaller than ours.

Happel & Bart (1974) reported a simple, square tank wall correction obtained with the method of reflections,

$$K = \frac{1}{1 - \dfrac{1.903266a}{L}}, \qquad [12]$$

which described the BEM prediction (and hence our experimental data) very well up to $a/L \approx 0.25$ only.

Basing the equivalent radius of a fictitious circular cylinder on the cross-sectional area of the square tank, we compared the established circular cylinder wall corrections of Bohlin (1960) and Haberman (1958) with our square tank data. As can be seen from figure 1, the agreement was very good with the former [being comparable with the Miyamura *et al.* (1981) correlation], while the latter was satisfactory only up to $a/L \approx 0.4$. In addition, the wall correction by Coutanceau (1971a,b) for a sphere falling in a circular cylinder shows remarkable agreement with the BEM and our experimental data over the whole range of sphere sizes.

The overall performance, in terms of the prediction error with respect to the experimental data, of the various wall corrections used for the square tube is summarized in table 3. It should be noted that the error associated with the BEM prediction of the experimental data presents an upper

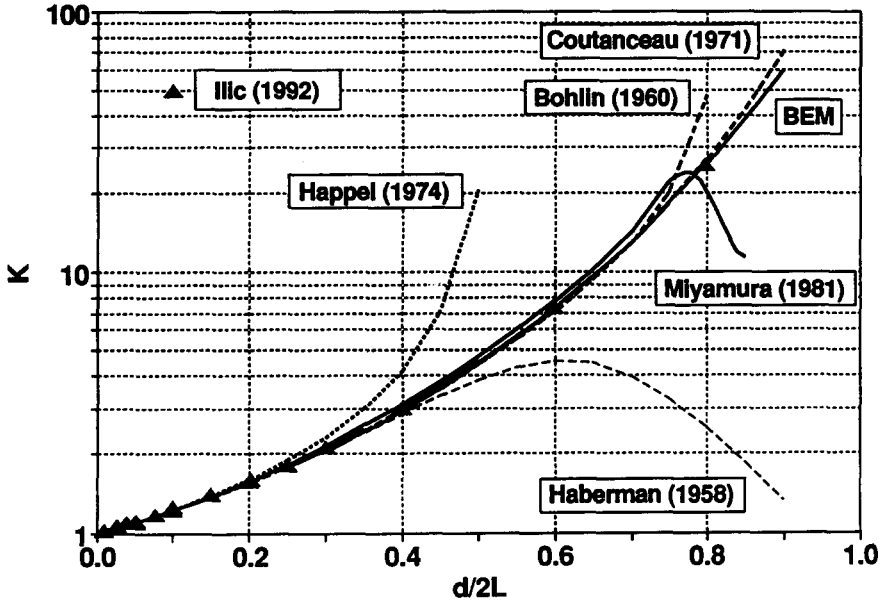

Figure 2. Comparison of estimates of the Stokes' law wall correction factor K—using the BEM, Bohlin (1960), Coutanceau (1971a,b), Haberman & Sayre (1958), Miyamura *et al.* (1981) and Happel & Bart (1974)—with the experimental data, Ilic (1992), in a square tube for a range of sphere sizes.

Table 2. Predicted and measured (present work) values of the Stokes' wall correction factor K for single spheres in a square tank falling along its axis

$d/2L$	a/R	BEM	Bohlin (1960)	Coutanceau (1971a,b)	Haberman & Sayre (1958)	Happel & Bart (1974)	Present work	Miyamura *et al.* (1981)
0.00000	0.000000		1.000000	1.000000	1.000000	1.000000	1.000000	1.00000
0.00945	0.008375		1.017939	1.017913	1.017944	1.018315	1.026162	1.01837
0.02490	0.022067		1.048675	1.048675	1.048689	1.049749	1.071010	1.04937
0.03780	0.033499		1.075753	1.075779	1.075775	1.077521	1.093793	1.07634
0.04990	0.044223		1.102394	1.102427	1.102424	1.104939	1.122760	1.10272
0.05000	0.044311	1.105665	1.102619	1.102652	1.102650	1.105172		1.10294
0.05040	0.044666		1.103522	1.103555	1.103552	1.106102	1.094162	1.10384
0.07495	0.066423		1.161671	1.161686	1.161720	1.166385	1.183157	1.16132
0.09960	0.088268		1.225976	1.226011	1.226040	1.233906	1.236191	1.22538
0.09970	0.088357		1.226250	1.226285	1.226314	1.234196	1.249522	1.22566
0.09995	0.088578		1.226935	1.226971	1.226999	1.234921	1.261395	1.22635
0.10000	0.088623	1.233259	1.227072	1.227108	1.227137	1.235066		1.22648
0.14971	0.132677		1.378127	1.378569	1.378142	1.39848	1.412292	1.38113
0.15000	0.132934	1.389657	1.379101	1.379548	1.379116	1.39956		1.38215
0.19960	0.176891		1.564690	1.565724	1.564212	1.612622	1.584979	1.58035
0.20000	0.177245	1.582932	1.566353	1.567390	1.565866	1.614604		1.58216
0.20160	0.178663		1.573033	1.574083	1.572514	1.622582	1.621045	1.58943
0.24975	0.221335		1.797848	1.798903	1.795257	1.905999	1.822508	1.83742
0.25000	0.221557	1.823955	1.799147	1.800200	1.796537	1.907729		1.83887
0.29980	0.265691		2.090305	2.090716	2.080766	2.328826	2.116703	2.16369
0.30000	0.265868	2.127610	2.091618	2.092025	2.082032	2.330893		2.16515
0.35000	0.310179	2.514592	2.463438	2.463570	2.433796	2.995295		2.57752
0.39880	0.353427		2.929441	2.931058	2.848748	4.149765	2.997593	3.09038
0.39980	0.354314		2.940294	2.941967	2.857994	4.182801	3.013578	3.10234
0.40000	0.354491	3.014102	2.942472	2.944156	2.859847	4.189471		3.10473
0.45000	0.398802	3.668289	3.568897	3.574676	3.354995	6.96717		3.80077
0.50000	0.443113	4.539075	4.401823	4.414035	3.881735	20.67525		4.75245
0.55000	0.487425		5.530680	5.553179	4.345277			6.06120
0.59884	0.530708		7.055334	7.099089	4.588865		7.341924	7.75644
0.60000	0.531736	7.353617	7.098241	7.142723	4.590845			7.80234
0.65000	0.576047	9.669627	9.362281	9.442540	4.473497			10.1566
0.70000	0.620359	13.041710	12.923150	12.906180	3.981407			14.1732
0.75000	0.664670	18.104530	19.917700	18.325760	3.264791			21.9874
0.79860	0.707741		45.864400	26.807860	2.536615		25.870880	20.5881
0.80000	0.708982	25.974810	47.860080	27.120040	2.516549			20.2335
0.85000	0.753293	38.693870		42.145040	1.859344			11.3973
0.90000	0.797604	60.142340		70.753140	1.332525			

bound, as it was based on the linear interpolation between adjacent experimental and calculated values of K for a given value of $d/2L$.

Table 3 shows that the BEM best described the experimental data, while the Miyamura *et al.* and Bohlin models were also good, except at large sphere diameters. Apart from the BEM, the Coutanceau model was the next best over the complete range of sphere sizes.

The magnitude of the experimental error expressed in terms of the fractional error in K, was typically of the order of the symbol size used in figure 2. Table 1 shows that the major component of this error was, typically, due to the uncertainty in the sphere size and liquid viscosity measurements.

The effect of eccentricity

For eccentrically dropped spheres in a circular and a square tank, the settling velocity was clearly influenced by the proximity of the container walls with, for the small sphere in a circular cylinder, a near constant settling velocity from the tank axis to about midway towards a wall, figure 3. A further increase in the eccentricity of the sphere drop resulted in a rapid decrease in the settling velocity within the proximity of the wall. However, for the large sphere, the settling velocity was much more strongly influenced by the eccentricity of the drop: apart from the region close to the tank axis ($b/R \approx 0.05$), the settling velocity was not constant, but increased with eccentricity to a peak at $b/R \approx 0.38$. For greater values of b/R, a rapid decrease in the settling velocity was apparent as for the small sphere. As the theoretical analysis of Happel & Brenner (1986) indicated, the drag for a small sphere in a circular cylinder does not increase monotonically in the outward direction from the cylinder axis towards the wall, but reaches a minimum. This radial variation of drag was reflected in varying settling velocity, figure 3. The agreement between the experimental data, the reflection solution and the BEM was excellent for the small sphere ($a/R = 0.107$). While the agreement between the experiment and BEM predictions was good for the large sphere ($a/R = 0.506$), the theoretical approach for the small sphere from Happel & Brenner (1986) was outside the range of applicability for this case.

For eccentric drops in a square cylinder, owing to excessive time requirements (several hours of CPU time per point on the Ardent Titan minicomputer) for the numerical simulation of this, only three point values were evaluated with the BEM. These values were non-dimensionalized with respect to the centerline velocity and tabulated with the experimental data in table 4.

Table 3. Percentage error $[100(K - K_{exp})/K_{exp}]$ in K relative to our experimental data

$d/2L$	BEM	Bohlin (1960)	Coutanceau (1971a,b)	Haberman & Sayre (1958)	Happel & Bart (1974)	Miyamura *et al.* (1984)
0.00945		−0.80	−0.80	−0.80	−0.76	−0.76
0.0249		−2.09	−2.09	−2.08	−1.99	−2.02
0.0378		−1.65	−1.65	−1.65	−1.49	−1.60
0.0499		−1.81	−1.81	−1.81	−1.59	−1.78
0.05	−1.02					
0.0504		0.86	0.86	0.86	1.09	0.88
0.07495		−1.82	−1.81	−1.81	−1.42	−1.85
0.0996		−0.83	−0.82	−0.82	−0.18	−0.87
0.0997		−1.86	−1.86	−1.86	−1.23	−1.91
0.09995		−2.73	−2.73	−2.73	−2.10	−2.78
0.1	−2.24					
0.14971		−2.42	−2.39	−2.42	−0.98	−2.21
0.15	−1.67					
0.1996		−1.28	−1.21	−1.31	1.74	−0.29
0.2	−0.58					
0.2016		−2.96	−2.90	−2.99	0.09	−1.95
0.24975		−1.35	−1.30	−1.50	4.58	0.82
0.25	−0.00					
0.2998		−1.25	−1.23	−1.70	10.02	2.22
0.3						
0.35						
0.3988		−2.27	−2.22	−4.97	38.44	3.10
0.3998		−2.43	−2.38	−5.16	38.80	2.95
0.59884		−3.90	−3.31	−37.50		5.65
0.7986	−0.45	77.28	3.62	−90.20		−20.42

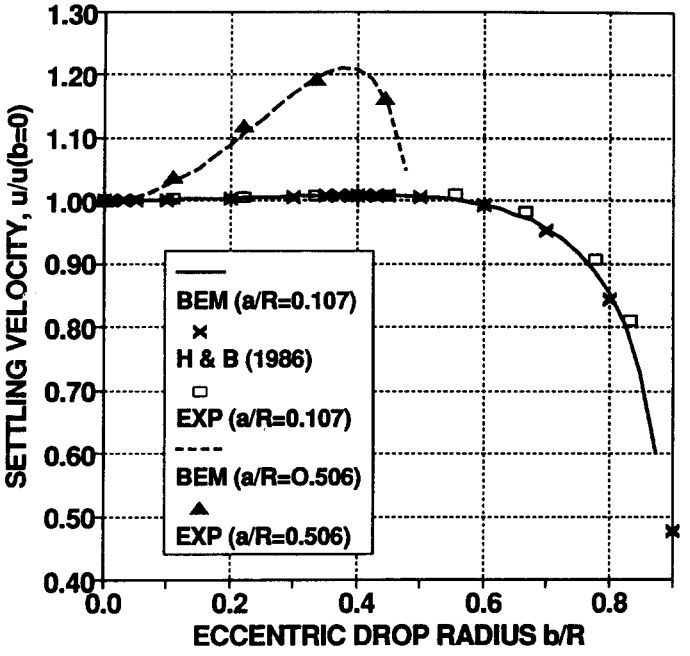

Figure 3. Variation of the dimensionless settling velocity $u/u(b=0)$ with the dimensionless drop distance b/R from the axis of a circular cylinder, 59.15 mm dia, for 6.35 and 29.95 mm dia spheres.

It is evident from the data that there is a qualitative agreement between the BEM predictions and the experimental values. Specifically, it is noted that the change in the sense of rotation for the small sphere was correctly predicted. An experimental error of about $\pm$ 17% was achieved for the angular velocity, while the settling velocity error was about $\pm$ 1% of the values quoted. These errors are associated with coordinate measurements from video tapes, resolution of the monitor screen, the finite thickness of the video pointer cursor and slight non-sphericity of the PMMA balls. Typically, the angular velocity determination required measurement of six vertically colinear coordinates compared to two for settling velocity. A density measurement of each sphere was made to ensure homogeneity of the material, and no attached air bubbles were seen on the sphere surface in the measurement section of the test cylinder. As can be seen from table 5, no rotation of the axially dropped spheres was observed in the square tank. The variation of angular velocity with drop radius, figure 4, is qualitatively similar to the behaviour of the associated settling velocity. Since rotation is purely shear driven, the sphere with the largest surface should be affected the most, as illustrated by the data. The small non-zero value of the angular velocity for the large sphere at the axis of the cylindrical tank is possibly caused by a small eccentricity of the axial drop. Large spheres are particularly sensitive to this, as Graham *et al.* (1989) noted.

It is also instructive to compare the experimental with the value of the "Newtonian standard" for $a/R = 0.500$ of the wall correction factor K for the large sphere settling axially in a cylinder—a

Table 4. Comparison of the predicted and measured settling and angular velocities of single PMMA spheres falling in a (50 x 50 mm) square tank at eccentric drop positions relative to the tank axis

	BEM		Experimental	
b/L	$U/U(b=0)$	$\omega a/U(b=0)$	$U/U(b=0)$	$\omega a/U(b=0)$
	(a) d = 6.40 mm, 2$2$ = 49.17 mm			
0.00000	1	-8.7×10^{-8}	1	0
0.50844	1.004573	0.008769	1.00226	0.004113
0.81350	0.845963	−0.01634	0.8344854	−0.001712
	(b) d = 12.85 mm, 2L = 49.17 mm			
0.00000	1	-1.6×10^{-8}	1	0
0.50844	1.018004	0.041157	1.002878	0.047785

case well-documented in Walters & Tanner (1992). They quoted the accepted standard value of K for $a/R = 0.500$ as 5.947, while the experimentally obtained value for $a/R = 0.506$ was 6.084. This appears to be reasonable, as increasing values of a/R imply, for a given cylinder, a larger and therefore heavier ball.

The end-surface effect

The effect of the end surface on sphere sedimentation along the axis of a square cylinder is shown in figure 5 in terms of normalized coordinates of sphere drop height $h(t)/h(t = T)$ and settling time $t(h = 0)/t(h = H)$, respectively. H and T denote the overall drop height and the time taken to traverse it, respectively. Two sets of data were considered: an aluminium sphere of 3.15 mm dia with $H = 34.3$ mm, $T = 63.27$ s; and a 30.00 mm dia Delrin sphere with $H = 43.5$ mm and $T = 27.28$ s. It is remarkable that the trajectories from the two different spheres collapse into one curve when normalized in the manner indicated above.

The essential feature of the data is that it showed a significant deviation from linearity at $t/T \approx 0.75$ and $h/H \approx 0.15$ for both spheres, as each sphere decelerated in the proximity of the end surface of the square cylinder. The deviation from linearity was also observed with single spheres settling along the axis of a circular cylinder and has been studied extensively (e.g. Brenner 1961; Tanner 1963; Sutterby 1973). Milne-Thompson (1979) showed that, for a laterally unbounded fluid, the decreasing velocity was associated with an increasing repulsion of the sphere from the end surface mandated by an overall energy balance.

While qualitatively similar, the BEM values were progressively higher than the experimental values of the drop height with increasing values of settling time. At $t/T = 0.8$ this discrepancy had grown to 100% and did not converge to zero at $t/T = 1.0$. This behaviour was not unexpected, however; first, the particle motion in the vicinity of the end surface is not purely Stokesian because it is essentially non-steady, as indicated by changing slope of the spheres' trajectory. However, it was considered that body and drag forces predominate, such that the inertial effects could be neglected in the numerical simulation. Secondly, problems arise in the numerical method from collocation points' overlap at the two mating surfaces, such that its solution has to be terminated at a finite separation between them. This distance can be reduced as much as practicable, however, with very dense meshing.

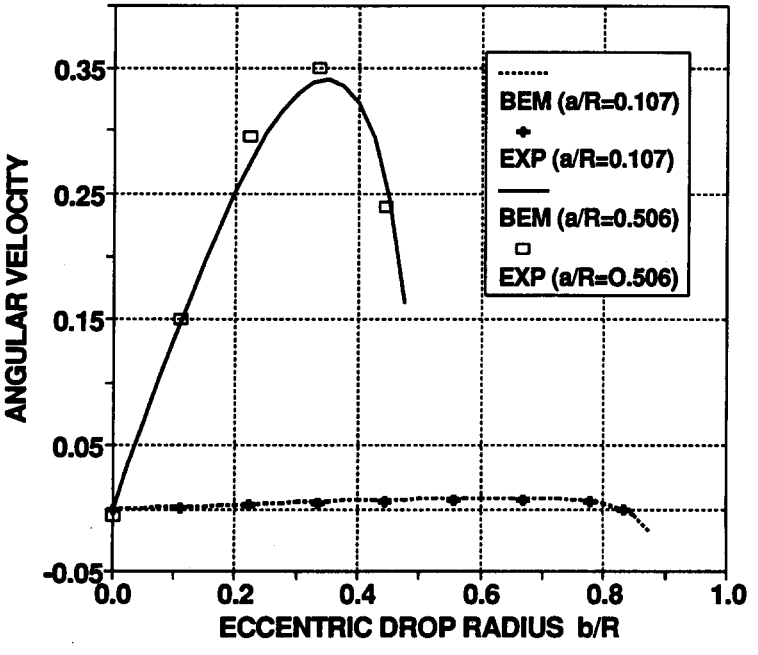

Figure 4. Variation of the dimensionless angular velocity of 6.35 and 29.95 mm dia spheres with the dimensionless drop distance from the axis of a circular cylinder 59.15 mm dia.

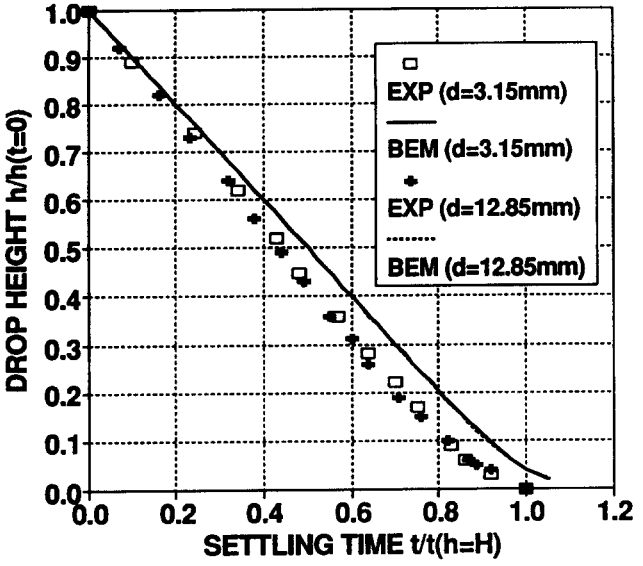

Figure 5. Trajectories of a 3.15 and 29.95 mm dia spheres in a square tank, 50 × 50 mm, in the vicinity of the end surface.

SUMMARY AND CONCLUSIONS

The terminal settling velocities and rotation rates of spherical particles settling in circular and square conduits were investigated experimentally and numerically. Spheres were allowed to settle in a viscous Newtonian fluid (silicone oil) such that only hydrodynamic forces exerted an appreciable effect. The terminal settling velocities and the rotation rates were measured as a function of the size and density of the falling sphere in the conduit over a wide range of experimental parameters. The experimental parameters were subjected to an exacting error analysis and compared with fully three-dimensional boundary element calculations. Within the bounds of experimental error, the experimental and numerical data showed remarkable agreement.

Specifically, the Stoke's law wall correction factor K was evaluated from settling velocity data of single spheres dropped axially in square tanks. The Bohlin and Haberman corrections, originally developed for circular cylinders, described the BEM data well up to $a/L \approx 0.75$ and 0.4, respectively, on the basis of equivalence of cross-sectional areas of the square tank and a fictitious cylinder. The correlation of Miyamura *et al.* (1981), developed specifically for a square tank, also agreed well with our BEM values for a/L up to ≈ 0.75, while the Happel & Bart (1974) correction, derived for a square tank, was only satisfactory for a/L values up to ≈ 0.25. The Coutanceau (1971a,b) correction showed remarkably good agreement over the whole range of sphere sizes.

The fully three-dimensional boundary element calculations showed good agreement, within the experimental error, with the data over the whole range of values of a/L.

Experimental data for eccentric drops in square and circular tanks were quantitatively similar and were described well with the boundary element calculations. Owing to radially varying shear, a half saddle-like shape of the settling velocity and rotational velocity was observed over the cylinder radius. Specifically, and in both cases, the centre of the trough was on the centreline of the tank, and the velocity peak (the magnitude of which increased with the particle size) was generally within $0.35 < b/L < 0.6$, where b denotes the radial displacement of sphere centroid from the conduit axis of symmetry. Velocities decreased rapidly in the proximity of the wall and, in the case of angular velocity, came close to zero for the point closest to the wall.

The settling velocity peak was greatest for the largest sphere size ($d/D = 0.506$), probably as a consequence of, among other things, steeper shear gradients than for the case of $d/D = 0.107$.

As a particle approached the end surface of a square tank, it decelerated before coming to rest at the tank bottom. The essential feature of the data is that it showed a significant deviation from linearity at $h/H \approx 0.15$ for both spheres, as each sphere decelerated in the proximity of the end

surface of the square cylinder due to increasing repulsion from the end surface. The BEM estimate of the height/time trajectory of a sphere approaching the end wall of a square cylinder showed a qualitative agreement with the experimental data. The BEM overpredicted the experimental trajectory of the settling spheres near the end surface of a square tank. This overprediction increased with settling time, such that it was about 100% at $t/T = 0.8$. The numerical value of h/H did not converge to zero at $t/T = 1.0$, but remained high. This was not unexpected, and is related to, among other things, the unsteady nature of the sedimentation velocity and limitations imposed by BEM, such as finite mesh size, close to the boundary surface.

It is interesting, however, that the sedimentation trajectories of the two disparate spheres near the end wall could be shown to collapse to approximately a single curve in a figure in which the sphere height was normalized with respect to the overall height, and the corresponding instant of time was normalized with respect to the overall time it took to traverse it.

As a continuation of this work, it is of interest experimentally to determine in detail how other particle shapes behave relative to a sphere in a similar set of experiments described here.

While the results of the reported work indicate that the BEM provides an excellent tool for modelling sedimentation of single spheres subject to Stokes' law in axisymmetric and fully three-dimensional configurations, further tests ought to be made in an attempt to reduce the experimental error margin below that reported here. This also applies to the discrepancy between the experimental and numerical results for the particle trajectory near the end surface in a square tank.

While single particle sedimentation data may be useful to applications in rheometry, the challenge of multiparticle sedimentation has a wider scope. In particular, the comparison of the BEM with experimental data, especially to elucidate the interparticle interaction would be of interest, though a more complex one to carry out experimentally, especially in concentrated systems.

Extension of this work to viscoelastic fluids would provide further physical insights, as well as a benchmark for developing and testing constitutive models and numerical techniques.

Acknowledgements—This work was supported by the University of Sydney Special Projects Grant and by the U.S. Department of Energy at Los Alamos National Laboratory under Contract W-7405-ENG-36 with the University of California. The authors gratefully acknowledge partial support for this work by the U.S. Department of Energy, Division of Engineering and Geosciences and Division of Material Science, Office of Basic Energy Sciences and through Dr R. S. Miller's section of the Mechanics Division of ONR. Portions of this work by Los Alamos National Laboratory was also supported by the Astronautics Laboratory (AFSC), Edwards AFB, California. The SKF Australia Pty Ltd supplied steel spheres.

REFERENCES

BACON, J. 1936 Measurement of absolute viscosity by the falling sphere method. *J. Franklin Inst.* **221,** 251–273.

BAGNOLD, R. A. 1954 Experiments on a gravity-free dispersion of large solid spheres in a Newtonian fluid under shear. *Proc. R. Soc. Lond.* **A225,** 49–63.

BANERJEE, P. K. & BUTTERFIELD, R. 1981 *Boundary Element Methods in Engineering Sciences.* McGraw-Hill, London.

BART, E. N. 1959 Interaction of two spheres falling slowly in a viscous medium. M.S. Thesis, New York Univ., NY.

BIRD, R. B., STEWART, W. E. & LIGHTFOOT, E. N. 1960 *Transport Phenomena.* Wiley International, New York.

BOHLIN, T. 1960 On the drag on a rigid sphere moving in a viscous liquid inside a cylindrical tube. *Trans. R. Inst. Technol. (Stockholm)* No. 155.

BREBBIA, C. A., TELLES, J. F. C. & WROBEL, L. C. 1984 *Boundary Element Techniques.* Springer-Verlag, Berlin.

BRENNER, H. 1961 The slow motion of a sphere through a viscous fluid towards a plane surface. *Chem. Engng Sci.* **16,** 242–251.

BRENNER, H. 1962 Dynamics of a particle in a viscous fluid. *Chem. Engng Sci.* **17,** 435–446.

BUSH, M. B. & TANNER, R. I. 1983 Numerical solution of viscous flows using integral equation methods. *Int. J. Numer. Meth. Fluids* **3,** 71–92.

CLIFT, R., GRACE, J. R. & WEBER, M. E. 1978 *Bubbles, Drops and Particles.* Academic Press, New York.

COUTANCEAU, M. 1968 Mouvement uniforme d'une sphère dans l'axe d'un cylindre contenant un liquide visqueux. *J. Méc.* **7,** 49–67.

COUTANCEAU, M. 1971a Contribution à l'étude théorique et expérimentalde l'écoulement d'un sphère qui se déplace dans l'axe d'un cylindre à faible nombre de Reynolds ou en règime irrotationnel. Thèse de doctorat d'etat, Univ. de Poitiers, France.

COUTANCEAU, M. 1971b Sur le calcul du champ hydrodynamique autour d'une sphère qui se déplace dans l'axe d'un écoulement de Poiseuille. *C.R. Acad. Sci. Paris* **273A,** 1097–1100.

COUTANCEAU, M. 1987 Confined creeping flow around an axisymmetry body: increase of the shape effect by a tube wall. *Fluid Dynam. Res.* **2,** 153–174.

CRAIG, F. F. 1951 Flow of fluids through fixed and expanded beds of spheres. Ph.D. Thesis, Univ. of Pittsburgh, PA.

FAXÉN, H. 1921 Ein wirkung der Gerfässuände auf den Widerstand gegen die Bewegung einer kleinen Kugel in einer zähen Flussigkeit. Dissertation, Upsala Univ., Sweden.

FIDLERIS, V. & WHITMORE, R. L. 1961 Experimental determination of the wall effect. Spheres falling axially in cylindrical vessels. *Br. J. Appl. Phys.* **12,** 490–494.

GRAHAM, A. L., MONDY, L. A., MILLER, J. D., WAGNER, N. J. & COOK, W. A. 1989 Numerical simulations of eccentricity and end effects in falling sphere rheometry. *J. Rheol.* **33,** 1107–1128.

HABERMAN, W. L. & SAYRE, R. M. 1958 David Taylor model basin Report No. 1143. U.S. Navy Dept, Washington, DC.

HAPPEL, J. & BART, E. 1974 The settling of a sphere along the axis of a long square duct at low Reynolds number. *Appl. Scient. Res.* **29,** 241–258.

HAPPEL, J. & BRENNER, H. 1986 *Low Reynolds Number Hydrodynamics.* Martinus Nijhoff, Boston, MA.

HIRSCHFELD, B. R., BRENNER, H. & FALADE, A. 1984 First- and second-order wall effects upon the slow viscous asymmetric motion of an arbitrarily-shaped, positioned and oriented particle within a circular cylinder. *PhysicoChem. Hydrodynam.* **5,** 99–133.

ILIC, V. 1992 Ph.D. Thesis (in progress), Dept of Mechanical Engineering, Univ. of Sydney, NSW.

LADENBURG, R. 1907 Influence of walls on sphere motion in a viscous medium. *Annln Phys.* **22,** 447–458 (in German).

LUNSMANN, W. J., BROWN, R. A. & ARMSTRONG, R. C. 1989 Summary of sphere in a tube calculations: UCM fluid. Private communication, Dept of Chemical Engineering, MIT, Cambridge, MA.

MILNE-THOMSON, L. M. 1979 *Theoretical Hydrodynamics,* 5th edn. Macmillan, New York.

MIYAMURA, A., IWASAKI, S. & ISHII, T. 1981 Experimental wall corrections factors of single solid spheres in triangular and square cylinders and parallel plates. *Int. J. Multiphase Flow* **7,** 41–66.

PLISKIN, I. & BRENNER, H. 1963 Experiments on the pressure drop created by a sphere settling in a viscous liquid. *J. Fluid Mech.* **17,** 89–96.

RIZZO, F. J. 1967 An integral approach to boundary value problem of classical elastostatics. *J. Appl. Math.* **25,** 83–95.

SHOEMAKER, D. P. & GARLAND, C. W. 1962 *Experiments in Physical Chemistry.* McGraw-Hill, New York.

SONSHINE, R. M., COX, R. G. & BRENNER, H. 1966a The Stokes translation of a particle of arbitrary shape along the axis of a circular cylinder filled to a finite depth with viscous liquid. I. *Appl. Scient. Res.* **16,** 273–300.

SONSHINE, R. M., COX, R. G. & BRENNER, H. 1966b. The Stokes translation of a particle of arbitrary shape along the axis of a circular cylinder filled to a finite depth with viscous liquid. II. *Appl. Scient Res.* **16,** 325–360.

STOKES, G. G. 1851 On the effect of the internal friction of fluids on the motion of pendulums. *Trans. Camb. Philos. Soc. Pt II* **9,** 8–27.

SUTTERBY, J. L. 1973a Falling sphere viscometry. I. Wall and inertial corrections to Stokes' law in long tubes. *Trans. Soc. Rheol.* **17,** 559–573.

SUTTERBY, J. L. 1973b. Falling sphere viscometry. II. End effects in short tubes Stokes' law in long tubes. *Trans. Soc. Rheol.* **17,** 575–585.

TACHIBANA, M. 1973 On the behaviour of a sphere in the laminar tube flows. *Rheol. Acta* **12,** 58–69.

TANNER, R. I. 1963 End effects in falling sphere viscometry. *J. Fluid Mech.* **17,** 161–170.

TOPPING, J. 1966 *Errors of Observation and Their Treatment.* Chapman & Hall, London.

TÖZEREN, H. 1982 Torque on eccentric spheres flowing in tubes. *Trans. ASME J. Appl. Mech.* **49,** 279–283.

TRAN-CONG, T. & PHAN-THIEN, N. 1986 Boundary element solution for half-space elasticity or Stokes problem with a no-slip boundary. *Comp. Mech.* **1,** 259–268.

TRAN-CONG, T. & PHAN-THIEN, N. 1989 Stokes' problems of multiparticle systems: a numerical method for arbitrary flows. *Phys. Fluids* **A1,** 453–461.

TULLOCK, D., PHAN-THIEN, N. & GRAHAM, A. 1992 Boundary element simulation of spheres settling in circular, square and triangular conduits. *Rheol. Acta.* In press.

WALTERS, K. & TANNER, R. I. T. 1992 The motion of a sphere through an elastic fluid. In *Transport Processes in Bubbles, Drops and Particles* (Edited by CHHABRA, R. P. & DE KEE, D.), pp. 73–86. Hemisphere, Washington, DC..

YOUNGREN, G. K. & ACRIVOS, A. 1975 Stokes flow past a particle of arbitrary shape: a numerical method of solution. *J. Fluid Mech.* **69,** 377–403.

ZHENG, R., PHAN-THIEN, N. & TANNER, R. 1990 On the flow past a sphere in a cylindrical tube: limiting Weissenberg number. *J. Non-Newton. Fluid Mech.* **36,** 27–49.